ACS APPLIED NANO MATERIALS

www.acsanm.org Letter

Pt Nanostructures Fabricated by Local Hydrothermal Synthesis for Low-Power Catalytic-Combustion Hydrogen Sensors

Dionisio Del Orbe Henriquez, Incheol Cho, Hyunwoo Yang, Jungrak Choi, Mingu Kang, Ki Soo Chang, Chan Bae Jeong, Sang Woo Han, and Inkyu Park*

Cite This: *ACS Appl. Nano Mater.* 2021, 4, 7−12 Read Online

ACCESS | Metrics & More | Article Recommendations | Supporting Information

ABSTRACT: Hollow, microrod-like Pt nanostructures are locally synthesized on a small, suspended microheater platform (9 μm × 110 μm) as the catalytic layer of a low-power hydrogen (H_2) catalytic combustion sensor. The Pt nanostructures are synthesized via two successive Joule heating-assisted chemical reactions. During operation, H_2 locally combusts on the surface of the Pt nanostructures and transfers heat to the microheater, which in turn changes its resistance. Because of the highly localized Pt nanostructures and the suspended microheater, the sensor exhibits high sensitivity ($\Delta R/R_0 \sim 0.46\%$ per percent of H_2), fast response and recovery speeds (<12 s), and low-power consumption (4 mW).

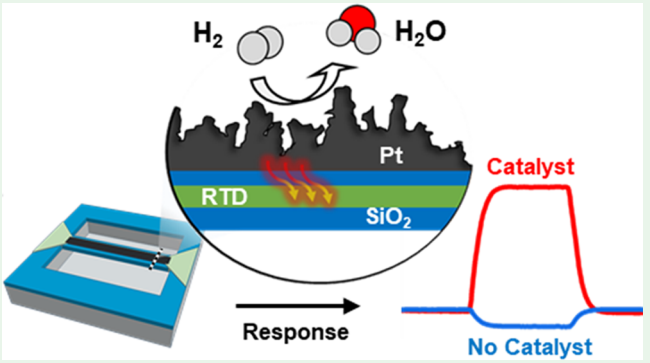

KEYWORDS: *Pt nanostructures, Pt catalyst, Hydrogen sensor, catalytic combustion, low power gas sensor, micromachined pellistor, MEMS, microheater*

The detection of hydrogen (H_2) gas, as a clean energy source, has become increasingly important as this odorless gas poses safety risks because of its explosive nature; it has a wide flammability range (4−75%) and requires a low ignition energy to combust. Chemiresistive gas sensors, operating based on the resistance changes of wide range of novel, nanostructured materials have been commonly used for the H_2 detection.[1−8] Also, catalytic combustion type gas sensors have been often used for the detection of combustible/flammable gases, like H_2 and CH_4, because of their good sensitivity toward combustible gases and low cost. However, the major drawback of catalytic combustion type gas sensors is that they operate at higher power levels, which limits their use in portable devices for mobile applications. With time, the conventional catalytic bead sensor evolved into MEMS-type catalytic combustion type sensors to reduce the power consumption of these sensors from several hundred mW to lower than 50 mW.[9−18] This modern MEMS-type catalytic combustion type sensor consists of an embedded microheater, usually made out of Pt, embedded in a suspended silicon dioxide or silicon nitride membrane. In general, on top of the membrane, a porous γ-Al_2O_3 layer (loaded with 5−30 wt % Pt or Pd) is drop-casted, which serves as a catalyst for the combustion of the target combustible gas and allows for the detection of the gas from the catalyst-promoted combustion.[11,12,18] Most of the limitations in reducing the power consumption of these devices arise from the large sizes of the typical γ-Al_2O_3 catalytic layers; previous research has exemplified the thermal, adhesion, and sensitivity issues of these conventional layers.[9]

Research has taken several routes to reduce the power consumption of modern MEMS-type catalytic combustion type sensors while attaining high sensitivity, fast response, and high selectivity. Particularly, researchers have focused on the development of microheater platforms that provide enough heat in a small area efficiently,[10,12] the syntheses of new catalytic layers that provide high catalytic responses,[9,10,13−16] and different integration methods (e.g., anodization,[9] electrodeposition,[10] screen printing,[16] and film deposition[17,18]) of the catalytic layer onto the microheater platform with good thermal contact and good overall response. While these studies have been successful in reducing the power consumption, a novel approach that combines all of these routes is needed to push the boundaries in attaining lower power consumption and superior performance of the devices. In-situ local integration methods through Joule heating has shown promise in this respect in chemiresistive devices.[19,20] Consistent with this idea, we have taken a three-pronged approach, which

Received: October 19, 2020
Accepted: November 30, 2020
Published: December 28, 2020

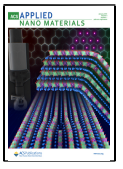

https://dx.doi.org/10.1021/acsanm.0c02794
ACS Appl. Nano Mater. 2021, 4, 7−12

includes a small, suspended microheater platform, highly catalytic nanomaterials, and local Joule heating for in situ hydrothermal integration of the catalytic nanomaterials onto the platform.

Specifically, in this Letter, we report the use of hollow, microrod-like Pt nanostructures (i.e., 70−80 wt % Pt) as a novel nanocatalyst, locally synthesized onto a small (9 μm × 110 μm) strip-type SiO_2 beam with an embedded Pt microheater for low-power H_2 detection. Here, the embedded microheater serves as a resistive temperature detector (RTD), which increases its resistance when H_2 combusts locally on the surface of the catalytic layer. To grow the Pt nanostructures, sputtered SnO_2 nanoparticles are used as seeds for the local hydrothermal growth of ZnO microrods through in situ Joule heating; this is an adaptation of the bulk synthesis of ZnO one-dimensional structures in the reference.[21] These microrods serve as scaffolds for the synthesis of the Pt nanostructures through a second hydrothermal process.[22] Before sputtering the SnO_2, a TiO_2 adhesion layer is deposited on the strip-type microheater to ensure good reliability and thermal contact of the catalytic layer.[23] Therefore, the high gas-sensing performance with low power consumption of the sensor, using these nanostructures with high catalytic activities, is demonstrated for H_2 sensing.

The fabricated catalytic combustion sensor consists of a strip-type, suspended SiO_2 beam with an embedded Pt microheater and Pt nanostructures on its surface as a catalytic layer; this is illustrated in Figure 1a. Figure 1b shows a

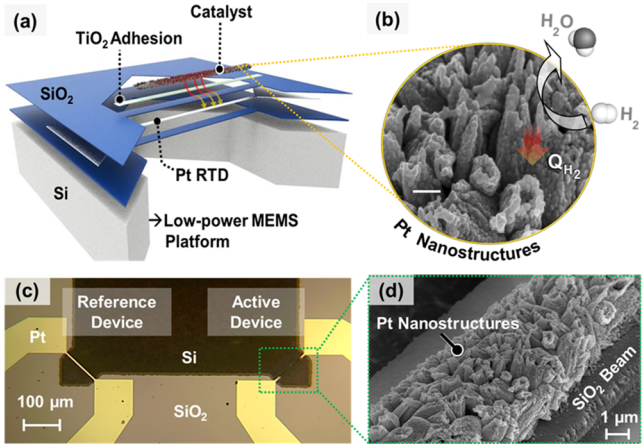

Figure 1. (a) Schematic representation of the low-power microheater platform with the integrated Pt nanostructures as the catalytic layer. (b) Scanning electron microscope (SEM) image of the Pt nanostructures alongside the catalyst-promoted combustion of H_2; the heat generated by this reaction is transferred to the underlying RTD, which changes its resistance by temperature rise. The scale bar is 500 nm. (c) Optical image of the reference and active devices. (d) SEM image of the synthesized nanostructures on the microheater platform (at a 45°-tilt angle).

schematic representation of the catalyst-promoted reaction of H_2 on the surface of the catalyst, which releases heat and increases the resistance of the embedded RTD by temperature rise. Figure 1c shows an optical image of the constructed device with the catalytic layer (right) and an additional, identical SiO_2 beam without the catalytic layer (left); they are referred to as the active device and the reference device, respectively. The reference device, separated from the active device by a distance of 400 μm to avoid thermal crosstalk, helps demonstrate the presence of the gas as its resistance, in contrast to the active device, decreases from the thermal cooling effect of the gas with a high thermal conductivity.

The fabrication of the platform follows standard photolithographic steps; the detailed description of the process is given in Figure S1. As both active and reference devices are suspended, they have greater thermal isolation from the substrate, thus minimizing heat loss and effectively reducing the power needed. This platform is a modified version of the platform in previous work used for chemiresistive-type gas sensors.[24,25]

To locally integrate the Pt nanostructures onto the platform, as shown in Figure 2a, three steps were followed: sputtering of

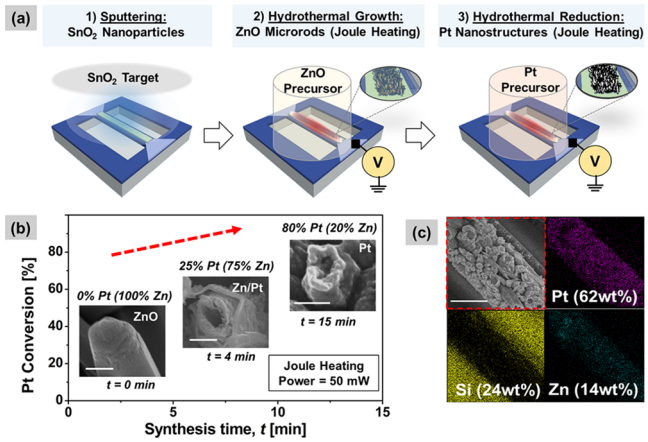

Figure 2. (a) Schematic representation of the integration of the Pt nanostructures (for the active device) onto the suspended microheater, based on a sputtering step and two sequential hydrothermal steps. (b) Morphological and elemental changes of the ZnO microrods into Pt nanostructures, as a function of synthesis time (in the final hydrothermal process with the Pt precursor); the scale bar is 500 nm. (c) EDS mapping of the suspended beam with the integrated Pt nanostructures. The scale bar is 5 μm.

SnO_2 nanoparticle seeds, hydrothermal growth of ZnO microrods, and conversion of these ZnO microrods into pseudoporous Pt nanostructures through the reduction of a metal salt. In short, after sputtering the SnO_2 seeds, Joule heating is applied to the microheater while it is submerged in a ZnO precursor using a polydimethylsiloxane (PDMS) well; the applied Joule heating promotes the growth of the ZnO microrods.[24,26] For the final step, the precursor solution is changed to an aqueous solution of potassium tetrachloroclatinate (mixed with a reducing agent) and Joule heating is applied to obtain the Pt nanostructures.[22] The input power for both hydrothermal processes is 50 mW; at this power, the surface of the device is a few degrees below 100 °C, a temperature needed for both hydrothermal processes. This process for the integration of the nanostructures is illustrated and explained in detail in Figure S2. The resulting Pt nanostructures are composed of hollow microrod-like structures with a rough surface resembling interconnected nanoparticles with diameters mostly between 30 and 80 nm (Figure S3).

Figure 2b shows the morphological and elemental changes in the final hydrothermal step. Here, ZnO is etched away slowly as the Pt gets reduced on the surface, promoted by the Joule heating. This mechanism has been previously explained in literature.[22] The final morphology shows hollow microrod-like structures with a pseudoporous nature. This structure is

https://dx.doi.org/10.1021/acsanm.0c02794
ACS Appl. Nano Mater. 2021, 4, 7−12

especially beneficial for gas sensing applications because of its increased surface area and easy gas diffusion. The final composition of the catalytic layer is mostly Pt as shown in Figure 2b and c from energy-dispersive X-ray spectroscopy (EDS) analysis. To investigate the atomic arrangement and elemental composition of the fabricated Pt nanostructures, a bulk process, using similar parameters to the in situ integration, was used for the transmission electron microscopy (TEM) and EDS analysis. Figure S4 shows the composition of a ZnO microrod-like structure converted to Pt nanostructures with a uniform Pt composition and a polycrystalline structure.

The proposed local hydrothermal synthesis of the Pt nanostructures in this work is comparable with the wafer-scale integration, for potential mass production, through the use of individual polymeric wells or polymeric microchannels connected to wells to guide and to contain different precursor solutions. The wafer-scale, parallel integration of ZnO nanowires has been demonstrated in the past with similar results between samples.[27] A more refined approach for greater throughput involves the use of polymeric microchannels connected to wells.[28] With the latter approach, sequential and parallel hydrothermal syntheses can be performed; thus, this method can be used to synthesize not only Pt but also Pd and other catalytic materials simultaneously.

As the constructed device relies on the transfer of heat to the underlying RTD to sense the presence of the gas, it is important to estimate both the temperature at which the device operates at and the heat that is produced during the local combustion of H_2. To do this, we used infrared microthermography, following the technique reported in the ref 29; Figure S5 explains the procedure for the temperature measurement. Specifically, an infrared (IR) camera was used to measure the irradiated energy off the beam when an increasing amount of Joule heating power is applied. In a separate step, this energy could be related to the actual temperature reading following a calibration step with a high-emissivity paint. Figure 3a shows the measured temperature with an increasing power. The top horizontal axis reads the corresponding resistance value at a given power. The linear fit between resistance (R) and power (P) is plotted in Figure S6. The linear fit shown in Figure 3a between the temperature and resistance readily relates the changes in resistance to the changes in temperature. The data plotted in this figure corresponds to the average temperature measured for a total of 3 devices. The standard deviation error bars shown, are small (a few °C), and may not be visible on the graph due to the other data points. As there may be some nominal differences of a few ohms between devices, this equation is meant to relate the changes in temperature to the changes in resistance ($\Delta T = 21.218^*\Delta R$). The device is operated at 4 mW for reasons that will be explained later. The IR temperature profile (top view) of a microheater, operated at 4 mW, is shown in the inset of Figure 3a.

The device was exposed to various concentrations of H_2 up to 1.6%, which is 40% of its lower explosive limit (LEL). This concentration is commonly used to trigger alarms for high levels of H_2. The schematic representation of the gas sensing setup is shown in Figure S7. The changes in resistance to the various concentrations is shown in Figure 3b. The resistance of active device increases, due to the generated heat during the local catalytic combustion, while the resistance of the reference device decreases because of the enhanced thermal cooling by H_2 with higher thermal conductivity than air by ~7 times. It is

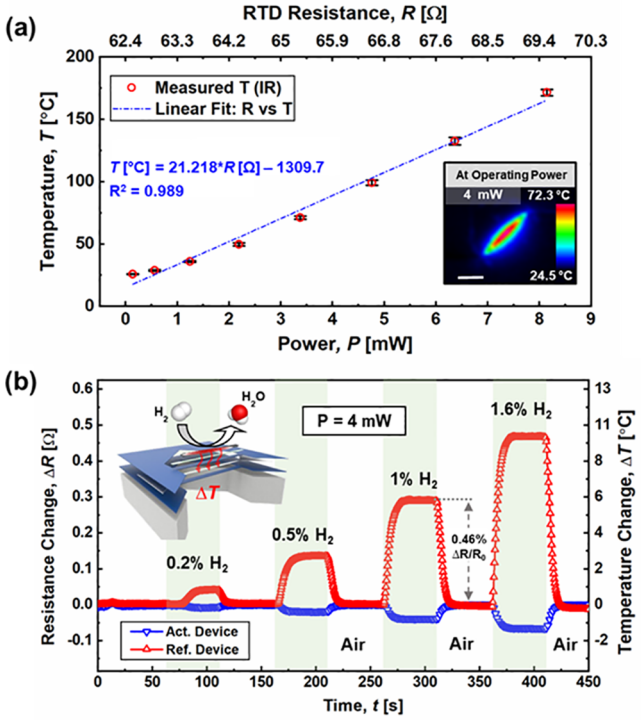

Figure 3. (a) Temperature of the surface of the microheater as a function of Joule-heating power, obtained through infrared micro thermography. As the power is increased, the resistance of the microheater increases (top x-axis). The linear fit relates the measured temperature changes to resistance changes. The inset shows the top, thermal distribution of the surface temperature of the microheater at 4 mW; the scale bar is 50 μm. (b) Resistance changes of the active and reference devices to various H_2 concentrations. The right y-axis displays the corresponding temperature increases produced during the combustive reaction.

noteworthy to mention that, in Figure 3b, we plot the changes in resistance values (ΔR), which can be directly related to the temperature changes in the right y axis. The response of the device is $\Delta R/R_0 \sim 0.46\%$ per percent of H_2, which corresponds to approximately 6 °C increase in the temperature. For 1% H_2, the 90% response and recovery times for the active device are, 11 and 10 s, respectively; for the reference device, these times are 10 (response) and 9.5 s (recovery). This speed, however, is thought to be influenced by the transient time of the gas from the mass flow controller to the chamber, as the chamber takes approximately 12 s to fill at a flow rate of 500 sccm. Most importantly, to the best of our knowledge, the proposed sensor is the lowest power under constant voltage operations for a catalytic combustion H_2 gas sensor developed to date.[11,14] We attribute this to the high catalytic activity of the catalytic layer, highly localized synthesis of catalytic Pt nanostructures, and suspended microheater structure. We have also included the real time, transient resistance of both devices in Figure S8a, along with the H_2 concentration versus response of the sensor Figure S8b. From this figure, we can see a high degree of linearity of the sensor which may serve for accurate estimation of target gas concentration during the sensor operation. This linear behavior is consistent with the reports on other catalytic gas sensors for various combustible gases.[9,11,13,14,16] Specifically, we expect a linear response from our sensor with respect to the concentrations up to 100% of the LEL of H_2. This is because

https://dx.doi.org/10.1021/acsanm.0c02794
ACS Appl. Nano Mater. 2021, 4, 7−12

our Pt microheater (our RTD) translates temperature increases linearly to resistance changes, and because our sensor is operated in the diffusion-limited region. Catalytic combustion gas sensors are operated in the diffusion-limited region by raising the temperature of the catalyst to a point where there are not significant changes of the output with temperature for a given gas concentration;[30] this is explained further in Figure 4.

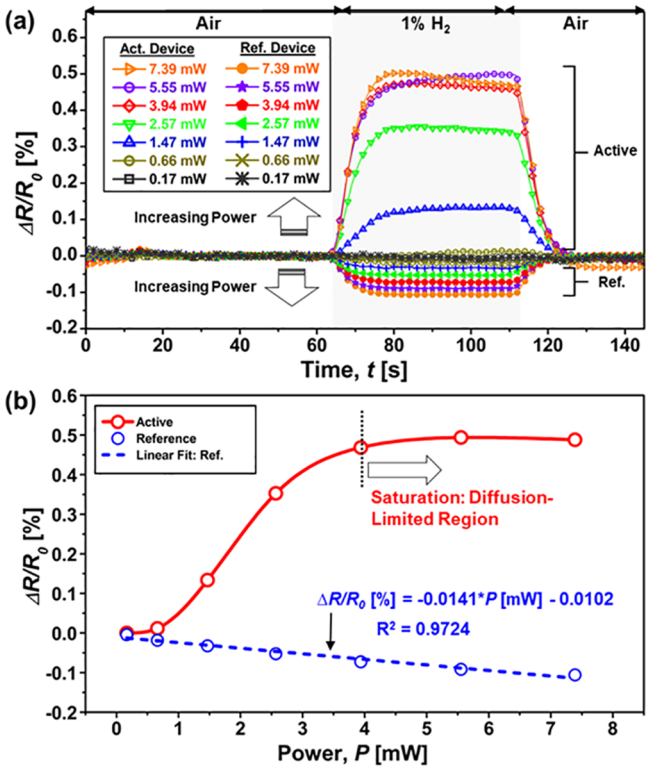

Figure 4. (a) Response of the active and reference devices to 1% H_2 as a function of power. (b) Reference device exhibits linear decreases in resistance from thermal cooling while the active device shows the catalytic light-off curve of a combustive reaction. This curve is characteristic of a gas/concentration/device system; thus, it may be utilized for identification of the gas. As the response saturates after 4 mW, this power is used for all the tests in this report.

For a catalytic combustion type gas sensor, when we vary the input power in the presence of the target combustible gas, we may see how the response changes with increasing power. If the activity of the catalyst is high and good thermal contact is ensured, the response saturates at a certain power (Figure 4a). For maximum response and lowest power, we want to operate our sensor at this power level; this is ∼4 mW for our sensor. Furthermore, the power versus response plot is a characteristic of a certain gas at a certain concentration that may help the identification of the gas; this is plotted in Figure 4b. The data shown in Figure 4b corresponds to the average response of the same reference and active devices shown in Figure 4a. This graph also shows that, after saturation, the response of the sensor starts decreasing slightly (after ∼6 mW). This behavior is commonly observed in catalytic gas sensors, as the absorption of oxygen on the catalyst decreases after a certain temperature.[14,16]

Additionally, we conducted further gas tests for humidity influences, repeatability, and selectivity (to H_2) of our sensor. Figure S9 shows the influence of different humidity levels to the response of our sensor. The reference device does not experience significant changes to humidity while the active device decreases linearly with increasing humidity levels; this variation with humidity may be compensated with the aid of an external humidity sensor. In another experiment (Figure S10), we tested the repeatability of the active device to repeated cycles of high concentration H_2 (1.6% H_2). The sensor shows a very stable response with minimal drift. Finally, in Figure S11, we explored the response of our sensor, not only to H_2 but also to other flammable/toxic gases (160 ppm of CO and 0.1% Acetone); these are concentrations close to the permissible exposure limits (PEL) of each gas/vapor. As previously explained, for the detection of gases through catalytic combustion, distinctive responses between the active and reference devices ought to be observed. For CO, the changes in the resistances of both the reference and active devices of our sensor are very small, indicating the absence of combustion or even significant thermal cooling (or heating). When exposed to acetone, both the active and reference devices show resistance increase (i.e., temperature increase) because of the low thermal conductivity of the acetone. Therefore, the selectivity of our sensor can be realized by analyzing the response patterns of active and reference devices by signal processing techniques such as machine learning. Also, if both the reference and active devices are arranged in a Wheatstone bridge configuration, only H_2 would show a signal voltage output. This selectivity of H_2 catalytic combustion type gas sensors against other flammable/toxic gases, with higher molecular weights, have been previously reported as H_2 is easier to catalytically combust at lower temperature ranges.[11,14,31] Thus, the selective detection of our catalytic combustion type gas sensor has been demonstrated for H_2 detection.

In summary, we have presented in this work the local hydrothermal synthesis of hollow, microrod-like Pt nanostructures as a new integration method for the catalytic layer of a low-power catalytic combustion type H_2 sensor. The Pt nanostructures are integrated onto a suspended MEMS microheater following a two-step local hydrothermal process through Joule heating. In the first step, ZnO microrods are locally grown on the surface of the microheater; in the second step, the microrods are converted into hollow microrod-like Pt nanostructures, with increased surface area, through the reduction of a Pt salt on the surface of the ZnO microrod scaffolds, which are simultaneously dissolved in the synthesis process. The highly localized integration allowed for the operation of our H_2 sensor at a very low power (4 mW) and allowed for our sensor to perform at fast response and recovery speeds (<12 s) with good sensitivity ($\Delta R/R_0$ ∼ 0.46% per percent of H_2) and with high selectivity. Given these characteristics and the increasing need to monitor combustible gases for industrial and personalized applications, the current device demonstrates its potential for battery-driven applications, especially in the advent of the Internet of things (IoT) era. To our knowledge, this constitutes the lowest constant-power for a catalytic combustion H_2 gas sensor. This is significant given that there is a consistent trend in the reference literature where smaller active areas is related to lower operating power for the different sensors;[9−18] thus, we expect the proposed method in this work presents a new approach for the integration of catalytic layers that may contribute to even lower power. Furthermore, our future work will include the

https://dx.doi.org/10.1021/acsanm.0c02794
ACS Appl. Nano Mater. 2021, 4, 7−12

synthesis of other noble catalytic materials and porous nanostructures for multiplexed gas sensing, the reduction in size of the platform and of the integrated catalytic nanostructures, and the application of pulsed heating for lower power consumption.

■ ASSOCIATED CONTENT

Supporting Information

The Supporting Information is available free of charge at https://pubs.acs.org/doi/10.1021/acsanm.0c02794.

Device fabrication, further material characterization; calibration of RTD for temperature estimation, gas testing setup, and additional gas sensing tests, humidity, repeatability, and selectivity (PDF)

■ AUTHOR INFORMATION

Corresponding Author

Inkyu Park − *Department of Mechanical Engineering, KAIST, Daejeon 34141, Republic of Korea;* orcid.org/0000-0001-5761-7739; Email: inkyu@kaist.ac.kr

Authors

Dionisio Del Orbe Henriquez − *Department of Mechanical Engineering, KAIST, Daejeon 34141, Republic of Korea;* orcid.org/0000-0002-1528-673X

Incheol Cho − *Department of Mechanical Engineering, KAIST, Daejeon 34141, Republic of Korea*

Hyunwoo Yang − *Department of Chemistry, KAIST, Daejeon 34141, Republic of Korea*

Jungrak Choi − *Department of Mechanical Engineering, KAIST, Daejeon 34141, Republic of Korea*

Mingu Kang − *Department of Mechanical Engineering, KAIST, Daejeon 34141, Republic of Korea*

Ki Soo Chang − *Center for Scientific Instrumentation, Korea Basic Science Institute, Daejeon 34133, Republic of Korea*

Chan Bae Jeong − *Center for Scientific Instrumentation, Korea Basic Science Institute, Daejeon 34133, Republic of Korea*

Sang Woo Han − *Department of Chemistry, KAIST, Daejeon 34141, Republic of Korea;* orcid.org/0000-0001-5406-5211

Complete contact information is available at: https://pubs.acs.org/10.1021/acsanm.0c02794

Notes

The authors declare no competing financial interest.

■ ACKNOWLEDGMENTS

This work was supported by the Development of Management Technology for HNS Accident (D11502815H480000140 2015034016), funded by the Ministry of Oceans and Fisheries, Korea. It was also supported by the Multi-Ministry Collaborative R&D Program (Development of Techniques for Identification and Analysis of Gas Molecules to Protect against Toxic Substances) through the National Research Foundation of Korea (NRF) funded by KNPA, MSIT, MOTIE, ME, and NFA (Grant NRF2017M3D9A1073858).

■ REFERENCES

(1) Cho, H. J.; Chen, V. T.; Qiao, S.; Koo, W. T.; Penner, R. M.; Kim, I. D. Pt-Functionalized PdO Nanowires for Room Temperature Hydrogen Gas Sensors. *ACS sensors* **2018**, 3 (10), 2152−2158.

(2) Yun, J.; Ahn, J. H.; Moon, D. I.; Choi, Y. K.; Park, I. Joule-Heated and Suspended Silicon Nanowire Based Sensor for Low-Power and Stable Hydrogen Detection. *ACS Appl. Mater. Interfaces* **2019**, *11* (45), 42349−42357.

(3) Lu, C.; Chen, Z. High-temperature resistive hydrogen sensor based on thin nanoporous rutile TiO_2 film on anodic aluminum oxide. *Sens. Actuators, B* **2009**, *140* (1), 109−115.

(4) Zhu, J.; Cho, M.; Li, Y.; Cho, I.; Suh, J. H.; Orbe, D. D.; Park, I.; et al. Biomimetic turbinate-like artificial nose for hydrogen detection based on 3D porous laser-induced graphene. *ACS Appl. Mater. Interfaces* **2019**, *11* (27), 24386−24394.

(5) Al-Hardan, N. H.; Abdullah, M. J.; Aziz, A. A. Sensing mechanism of hydrogen gas sensor based on RF-sputtered ZnO thin films. *Int. J. Hydrogen Energy* **2010**, *35* (9), 4428−4434.

(6) Cho, M.; Zhu, J.; Kim, H.; Kang, K.; Park, I. Half-Pipe Palladium Nanotube-Based Hydrogen Sensor Using a Suspended Nanofiber Scaffold. *ACS Appl. Mater. Interfaces* **2019**, *11* (14), 13343−13349.

(7) Gao, M.; Cho, M.; Han, H. J.; Jung, Y. S.; Park, I. Palladium-decorated silicon nanomesh fabricated by nanosphere lithography for high performance, room temperature hydrogen sensing. *Small* **2018**, *14* (10), 1703691.

(8) Hübert, T.; Boon-Brett, L.; Black, G.; Banach, U. Hydrogen sensors-a review. *Sens. Actuators, B* **2011**, *157* (2), 329−352.

(9) Bársony, I.; Ádám, M.; Fürjes, P.; Lucklum, R.; Hirschfelder, M.; Kulinyi, S.; Dücső, C. Efficient catalytic combustion in integrated micropellistors. *Meas. Sci. Technol.* **2009**, *20* (12), 124009.

(10) Lee, S. M.; Dyer, D. C.; Gardner, J. W. Design and optimization of a high-temperature silicon micro-hotplate for nanoporous palladium pellistors. *Microelectron. J.* **2003**, *34* (2), 115−126.

(11) Lee, E. B.; Hwang, I. S.; Cha, J. H.; Lee, H. J.; Lee, W. B.; Pak, J. J.; Ju, B. K.; et al. Micromachined catalytic combustible hydrogen gas sensor. *Sens. Actuators, B* **2011**, *153* (2), 392−397.

(12) Xu, L.; Wang, Y.; Zhou, H.; Liu, Y.; Li, T.; Wang, Y. Design, fabrication, and characterization of a high-heating-efficiency 3-D microheater for catalytic gas sensors. *J. Microelectromech. Syst.* **2012**, *21* (6), 1402−1409.

(13) Harley-Trochimczyk, A.; Pham, T.; Chang, J.; Chen, E.; Worsley, M. A.; Zettl, A.; Maboudian, R.; et al. Platinum Nanoparticle Loading of Boron Nitride Aerogel and Its Use as a Novel Material for Low-Power Catalytic Gas Sensing. *Adv. Funct. Mater.* **2016**, *26* (3), 433−439.

(14) Harley-Trochimczyk, A.; Chang, J.; Zhou, Q.; Dong, J.; Pham, T.; Worsley, M. A.; Mickelson, W.; et al. Catalytic hydrogen sensing using microheated platinum nanoparticle-loaded graphene aerogel. *Sens. Actuators, B* **2015**, *206*, 399−406.

(15) Yasuda, K. E.; Visser, J. H.; Bein, T. Molecular sieve catalysts on microcalorimeter chips for selective chemical sensing. *Microporous Mesoporous Mater.* **2009**, *119* (1−3), 356−359.

(16) Han, C. H.; Hong, D. W.; Kim, I. J.; Gwak, J.; Han, S. D.; Singh, K. C. Synthesis of Pd or Pt/titanate nanotube and its application to catalytic type hydrogen gas sensor. *Sens. Actuators, B* **2007**, *128* (1), 320−325.

(17) Cavicchi, R. E.; Poirier, G. E.; Tea, N. H.; Afridi, M.; Berning, D.; Hefner, A.; Montgomery, C.; et al. Micro-differential scanning calorimeter for combustible gas sensing. *Sens. Actuators, B* **2004**, *97* (1), 22−30.

(18) Liu, X.; Dong, H.; Xia, S. Micromachined catalytic combustion type gas sensor for hydrogen detection. *Micro Nano Lett.* **2013**, *8* (10), 668−671.

(19) Yang, D.; Fuadi, M. K.; Kang, K.; Kim, D.; Li, Z.; Park, I. Multiplexed gas sensor based on heterogeneous metal oxide nanomaterial array enabled by localized liquid-phase reaction. *ACS Appl. Mater. Interfaces* **2015**, *7* (19), 10152−10161.

(20) Kim, D.; Yang, D.; Kang, K.; Lim, M. A.; Li, Z.; Park, C. O.; Park, I. In-situ integration and surface modification of functional nanomaterials by localized hydrothermal reaction for integrated and high performance chemical sensors. *Sens. Actuators, B* **2016**, *226*, 579−588.

(21) Da Silva, L. F.; Lopes, O. F.; Catto, A. C.; Avansi, W.; Bernardi, M. I.; Li, M. S.; Longo, E.; et al. Hierarchical growth of ZnO nanorods over SnO_2 seed layer: insights into electronic properties from photocatalytic activity. *RSC Adv.* **2016**, *6* (3), 2112−2118.
(22) Lee, Y. W.; Lim, M. A.; Kang, S. W.; Park, I.; Han, S. W. Facile synthesis of noble metal nanotubes by using ZnO nanowires as sacrificial scaffolds and their electrocatalytic properties. *Chem. Commun.* **2011**, *47* (22), 6299−6301.
(23) Abe, N.; Otani, Y.; Miyake, M.; Kurita, M.; Takeda, H.; Okamura, S.; Shiosaki, T. Influence of a TiO_2 adhesion layer on the structure and the orientation of a Pt layer in $Pt/TiO_2/SiO_2/Si$ structures. *Japanese journal of applied physics* **2003**, *42* (5R), 2791.
(24) Cho, I.; Kang, K.; Yang, D.; Yun, J.; Park, I. Localized liquid-phase synthesis of porous SnO_2 nanotubes on MEMS platform for low-power, high performance gas sensors. *ACS Appl. Mater. Interfaces* **2017**, *9* (32), 27111−27119.
(25) Suh, J. H.; Cho, I.; Kang, K.; Kweon, S. J.; Lee, M.; Yoo, H. J.; Park, I. Fully integrated and portable semiconductor-type multi-gas sensing module for IoT applications. *Sens. Actuators, B* **2018**, *265*, 660−667.
(26) Greene, L. E.; Yuhas, B. D.; Law, M.; Zitoun, D.; Yang, P. Solution-grown zinc oxide nanowires. *Inorg. Chem.* **2006**, *45* (19), 7535−7543.
(27) Yang, D.; Kim, D.; Ko, S. H.; Pisano, A. P.; Li, Z.; Park, I. Focused energy field method for the localized synthesis and direct integration of 1D nanomaterials on microelectronic devices. *Adv. Mater.* **2015**, *27* (7), 1207−1215.
(28) Yang, D.; Kang, K.; Kim, D.; Li, Z.; Park, I. Fabrication of heterogeneous nanomaterial array by programmable heating and chemical supply within microfluidic platform towards multiplexed gas sensing application. *Sci. Rep.* **2015**, *5*, 8149.
(29) Chang, K. S.; Yang, S. C.; Kim, J. Y.; Kook, M. H.; Ryu, S. Y.; Choi, H. Y.; Kim, G. H. Precise temperature mapping of GaN-based LEDs by quantitative infrared micro-thermography. *Sensors* **2012**, *12* (4), 4648−4660.
(30) Miller, J. B. Catalytic sensors for monitoring explosive atmospheres. *IEEE Sens. J.* **2001**, *1* (1), 88−93.
(31) Brauns, E.; Morsbach, E.; Kunz, S.; Bäumer, M.; Lang, W. A fast and sensitive catalytic gas sensors for hydrogen detection based on stabilized nanoparticles as catalytic layer. *Sens. Actuators, B* **2014**, *193*, 895−903.

https://dx.doi.org/10.1021/acsanm.0c02794
ACS Appl. Nano Mater. 2021, 4, 7−12